 DOI: 10.3217/978-3-85125-954-4-05

Statistical shape modeling and analysis of the vestibular organ based on CT-images

Claudia Companioni Brito Matthias Willenbrink Karl Fritscher
Rainer Schubert
Private University of Health Sciences, Medical Informatics and Technology
Hall in Tirol, Austria

Abstract

The human body's stable posture and movement are dictated by the precise functioning of the vestibular organ, mainly the ampulla organs in the semicircular canals. The development of electronic devices such as vestibular implants aims to improve the vestibular system's capacity by stimulating the involved vestibular nerves. We aim to describe and analyze anatomical variations of the inner ear using computationally derived statistical shape models. The models should support the design process of vestibular implants. Based on a dataset of 81 cone-beam computed tomography, this work covers constructing a statistical shape model of the semicircular canals using a recently developed novel Particle-Based Modeling approach. The method optimally places correspondence points on each surface using a gradient descent energy function. Then Principal Component Analysis is used to describe anatomical variation. The model was evaluated in terms of reconstruction accuracy, compactness, generalization, and specificity. Results obtained by the workflow based on human datasets and the average shape of a statistical model revealed a high qualitative understanding and a quantitatively comparable range. The first three principal components captured 57.7% of the cumulative variation. The analysis led to 26 principal components to account for 95% of the total shape variation captured. The shape model can be used for virtual product development and testing and to estimate the detailed inner ear shape from a clinical patient computed tomography scan. For the first time, we could describe the geometry of the human semicircular canals based on a large sample of data from living humans compared with other studies.

1. Introduction

The human ear is the organ that enables hearing and balance. The anatomy of the human ear consists of three parts: the outer ear, the middle ear, and the inner ear. The vestibular system is the apparatus of the inner ear involved in balance. It is a complex organ consisting of three semicircular canals (superior/anterior, posterior, and horizontal/lateral) and the vestibule that houses the otolith organs. The most common medical complaints [24, 26] associated with imbalance symptoms include dizziness or vertigo. Among the vestibular disorders, benign paroxysmal positional vertigo (BPPV) is the most common cause of vertigo [26] which affects females twice as often as males [18]. Vestibular implants (VI) are a new promising technology based on the experiences of cochlear implants [14]. The vestibular nerves are the subject for electrical stimulation to treat balance disorders instead of the cochlear nerve. All the conditions leading to a loss of balance can be severely debilitating and cause a decrease in the quality of life [13, 23], so even though much research is still needed, the technology has a lot of potentials. Patient-specific 3D reconstruction of the vestibular system and its substructures could improve different aspects of vestibular implantation. It can facilitate anatomical understanding for doctors and suggest modifications in the design of electrode placement for vestibular implant manufacturers. To acquire surgical skills, lots of practice and effort are needed; thus, 3D models could be used for surgery simulation and training [10]. Quantitative analysis of the anatomical semicircular canal shape from medical images is essential for diagnosing shape abnormality. In this context, statistical shape models (SSM) turned out to be very useful for investigating variations of shape within anatomical structures of the inner ear. Statistical shape models describe and analyze the human anatomy and its variations, where the parameters of the probabilistic model have been learned from data [1, 7]. It has become an indispensable tool for medical image analysis. Moreover, having a shape model of the vestibular system could be further used for segmentation applications.

1.1. Related work

There are many applications concerning SSM of different anatomies (i.e., segmentation of brain and cardiac

structures, orthopedics, and other non-segmentation applications). However, few works applied SSM to analyzing the inner ear, most of which focus on the cochlea [6, 12, 16, 17]. The mathematical method developed by Bradshaw et al. automatically reconstructs the semicircular ducts from high-resolution computed tomography (CT) images in living humans [2] using a 2D B-spline contour. Noble et al. [18, 19] presented a point distribution model (PDM) based on micro-CT images along with an active shape model (ASM) approach to segment and predict preoperative CT datasets. The model is based on micro-CTs of cadaveric cochlea specimens with 36 µm voxel size. The scala tympani and scala vestibuli were manually segmented to create surface models. Point correspondences between the surfaces were generated using an image registration based on the Adaptive Bases algorithm [20]. In [16], Kjer et al. created an SSM of the human inner ear from micro-CT data. The cochlea and structures of the vestibular system were manually delineated based on 17 micro-CT scans of the human temporal bones. An initial alignment was applied to remove translational and rotational differences between the samples, followed by a multi-level B-Spline registration approach using bending energy regularization [21]. The resulting transformations were used to create a statistical PDM of the inner ear containing 16 modes of variation.

Fritscher et al. [11] introduced a framework for creating statistical shape and appearance models of the vestibular system for morphological analysis and the segmentation of the temporal bone. To find corresponding points across all subjects, a transformation consisting of two components: a global rigid transformation and a local deformable transformation, was applied [11]. The resulting deformation vector fields represented the shape variations among the training set and were the input for statistical analysis using Principal Component Analysis (PCA). Furthermore, the approach presented in [11] was extended to visualize and analyze novel multi-object models [19]. Based on the manual segmentation of 31 micro-CT datasets of temporal bones with an isotropic resolution of 15 µm, the SSMs for the following structures were created: Perilymph, Endolymph, Bony labyrinth (approximated using a combined label of endolymph and perilymph), N. ampullaris, N. singularis, N. facialis.

Recently, another approach for reconstructing semicircular canals (SCC) uses an automatic skeletonization process [8]. This approach is based on magnetic resonance imaging (MRI) scans of 20 individuals. The method computes the geometric parameters of the SCC through a skeletonization process of a binary image. The skeletonization approach uses potential field methods, which track field lines and potential valleys in a continuous space. Most of these works mentioned above are based on specimens from deceased subjects and have limited data for experiments. High-resolution images are obtained in cadaveric specimens after cropping the temporal bone around the bony labyrinth. The preparation and processing of ex-vivo specimens add consequent effort to acquiring the samples and potentially impact the data's quality and usability. While clinical CT images provide a less detailed representation of the inner ear, it is the best data source for living VI candidates. This study is based on existing clinical patient data, which is used in the regular routine of medical doctors that will, later on, use the VI. Therefore we wanted to take not artificially produced data but the kind of images used at the hospitals. The present work aims to develop and describe a detailed statistical shape model of the human SCC geometry based on an initial cohort of 81 subjects to serve as design decision support for a vestibular implant. Using a novel particle-based shape modeling approach facilitates the design of VI.

2. Materials and methods

2.1. Dataset

Eighty-one cone-beam computed tomography (CBCT) scans of human temporal bones used for this study were acquired from Maastricht University, from which 41 were from the left ear, and the rest were from the right ear. The age of the subjects ranged from 19 to 88 years, with an average age of 58.5 years. The group was divided into 44 men with an average age of 57.7 years and 37 women with an average of 59.3 years. The images in the dataset were acquired over a period of approximately ten years with different slice thicknesses. Some scans have a resolution of 0.4 mm and others 0.6 mm. The segmentations performed by medical experts include hearing bones, vestibular organs, and the facial nerve.

The dataset used in this work did not include abnormal anatomy. Exclusion criteria were applied due to missing CTs in the dataset, with only segmented labels available, and segmentations containing gaps in the canals. In total, 71 subjects were considered to create the SSM.

2.2. Statistical shape modeling

The approach presented by Cates et al. [4, 5] to establish correspondence has been used for the creation of the SSM. The general strategy of Particle-Based Modeling (PBM) is to represent correspondence points as interacting sets of particles, one for each shape, that redistribute themselves under an energy optimization and therefore describe the surface geometry [4]. The optimization function finds correspondence positions that minimize the entropy of the model. A more detailed description of the PBM method is referred to [5]. Since the vestibular system is a very complex structure, the PBM method suits well since its particle system formulation captures better-detailed areas by increasing the particle distribution rates in the higher curvature regions.

The PBM is defined as a collection of n shapes of k correspondence points. In our experiments, n is the number of SCC segmentations (n = 71), and k represents the number of landmarks used to describe each surface. The correspondences among the SCC segmentations are determined by running the PBM method to define a set of k correspondence landmarks x; where point xi on shape number 1 matches to point xi on shape 2, 3, 4,. . . , n and i = 1,. . . , k. Several experiments were carried out to set parameters for obtaining an optimal and detailed shape representation of the SCCs embedded in the bone structures of the inner ear. The final shape model of the SCC surface was constructed using 4096 correspondence particles per shape. This number of points was chosen by adding particles until the representation was able to recover anatomically plausible and accurate SCC shapes, and increasing this number did not reveal additional details. The experts quantitatively validated the final number of points for the surface representation at our research group (Institute of Biomedical Image Analysis) by visualizing and comparing the results with the given segmentations.

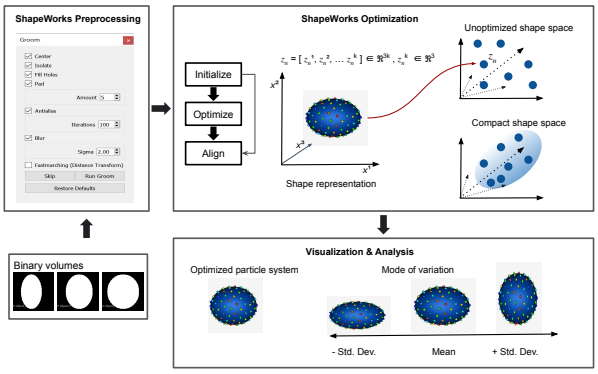

Figure 1. ShapeWorks pipeline. First, the binary segmentations need to be converted to signed DT using a set of grooming steps. After the ShapeWorks optimization stage, statistical analysis is performed using PCA. The mean and modes of shape variation are computed based on the optimized correspondence model. Image modified from [3].

This work uses an open-source distribution of the PBM algorithm called ShapeWorks [3], developed at the University of Utah. ShapeWorks is a publicly available tool with a pipeline of pre-processing steps required before computing the correspondence points. The optimization phase initializes the particle system and runs the PBM algorithm. It takes an initial set of particle positions and the processed data to the signed distance transform to construct the correspondence point model of shape Fig. 1. After the ShapeWorks Optimize step, we have a correspondence model for the population. Then, PCA was used to reduce the high dimensionality of the data matrix required to examine variation among the different SCC structures while still retaining most of the geometric information of the shapes. PCA isolated the modes of variation from the optimized correspondence particle locations. Once the m PCA modes that contain substantial variation are chosen, the model can represent every SCC shape in the set as an m-dimensional vector of scalar values. The shape variations are analyzed by examining the shape described by each principal component (PC), moving between ± 2 standard deviations from the mean in that PC.

3. Results

3.1. Data processing

The segmentation quality of the data was not sufficient, and manual clean-up was needed before using the dataset for further processing in the construction of the SSM (Figure 2a). Small holes and voxel-islands caused by manual segmentation were removed using a connected component analysis and morphological closing operation [25]. Then, the noticeable defects not eliminated by the pre-processing algorithms were corrected by hand using the 3D Slicer toolbox. Since the focus in this work is concerned with the SCCs, only the segmented labels, including it, were considered.

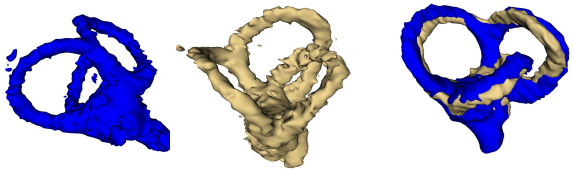

(a) (b)

Figure 2. 3D view of two dataset samples (a) before and (b) after pre-processing. All the segmentations were mirrored and aligned. Small holes and voxel-islands caused by manual segmentation have been removed using morphological operations.

All the right inner ears were mirrored so that all datasets appear to be of a left inner ear in order to obtain consistent data (Fig. 2b). First, a transformation including mirroring was calculated using the provided fiducial points in each semicircular canal and applied to all datasets on the right side. Next, all the datasets were aligned using a two-step registration process [25]. The fiducial points were used to apply for an initial rigid point base registration. Then, an additional rigid registration was applied using the former stage as initialization to avoid dependence on fiducials from unknown precision.

All images were resampled using linear interpolation with an isotropic voxel resolution of 0.15 x 0.15 x 0.15 mm.

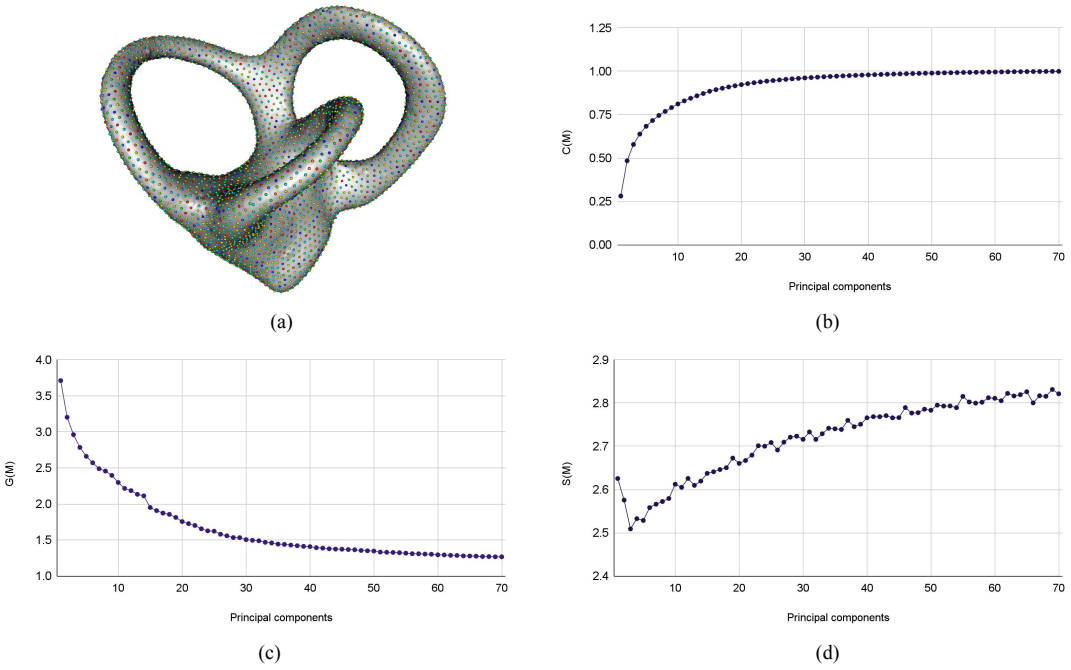

Figure 3. a) Mean shape. b) Compactness, c) Generalization, and d) Specificity of the SCC shape model.

The size was set to 300 x 300 x 300 voxel ROI spanning. At the time of writing, the selected SSM software in this study needed all the data with the same size, and the voxel spacing equals 1. Thus, the volumes were artificially scaled up by setting the spacing to 1.0 x 1.0 x 1.0 mm. More details about the registration and processing of the data can be found in [25].

3.2. Statistical shape model of the vestibular organ

The resulting mean shape after generating the SSM of the vestibular system using the PBM algorithm is visualized in Fig. 3a.

The vestibule's SSMs with different points were generated and analyzed, showing that poor reconstructions are observed with a smaller number of particles, especially along the canals. In our experiments, increasing the particle counts further than 4096 does not significantly improve the model's accuracy but increases the complexity of the model and computational time. The optimization routine using 4096 particles in a computer with 96 GB of RAM and an Intel Core i7 processor took approximately 7 hours. The duration of the optimization with 256, 1024, and 8192 particles was around 0.31, 1.3, and 14 hours respectively.

3.3. Principal component analysis

The PCA shape decomposition is able to represent 95% of the variation among SCC using 26 modes. The first three modes captured 57.7% of the cumulative variation among all shapes. Specifically, mode 1 captured 28.0% of the variation, followed by mode 2 at 20.3%, and mode 3 at 9.4%. Knowledge of the position of different datasets in PCA space is significant for identifying similar shapes and datasets that are close to the mean shape. Therefore, the PCs covering the highest amount of shape variation were used to analyze the distribution of the datasets in PCA space Fig. 4.

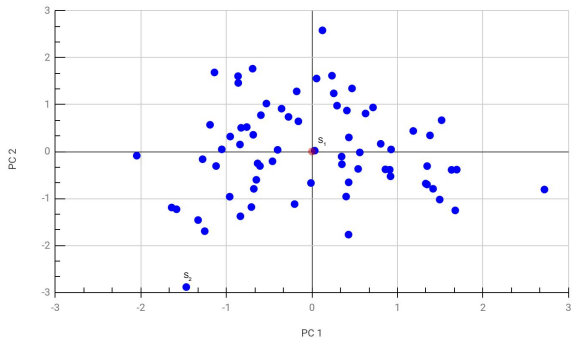

Figure 4. Distribution of input datasets with respect to PC1 and PC2. The red dot represents the mean shape. S_1 is the closest shape to the mean and S_2 is a random shape distant from the mean.

Shape variations of the first four modes were investigated to analyze the influence of specific PCs on the SSM. Fig. 5 shows the mean correspondence positions from the model

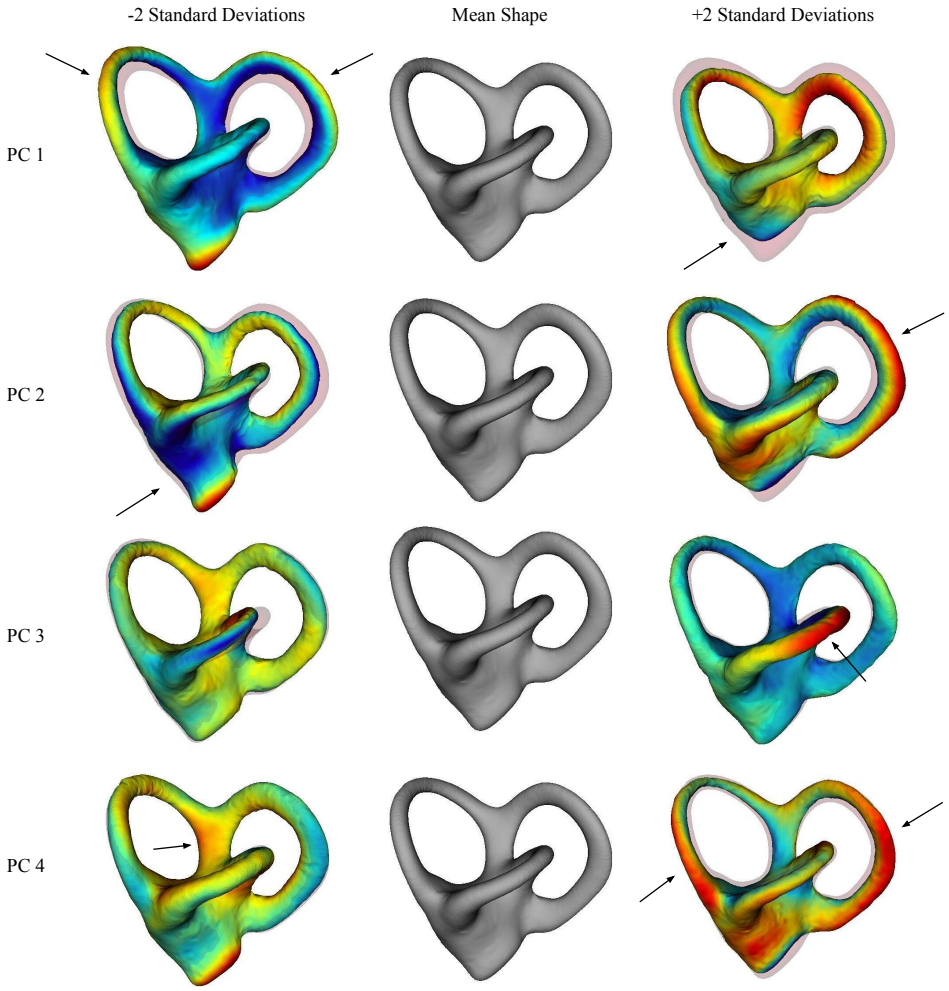

Figure 5. Influence of different PCs on the shape variation. The mean shape is in the center. In the left and right columns, deformation is represented as a color map, and the mean shape is visualized as opaque. The color maps represent the distance for any value inside the geometry with a negative value (blue) and outside the geometry with a positive value (red). The arrows highlight some relevant parts of the shape variations.

moved along each of the top four PCA modes. SCC shapes along each mode are reconstructed from the learned PBM model parameters at –2 to +2 standard deviations from the mean.

From Fig. 5, we can interpret that the first PC causes size changes of the SCC. Variation in a positive direction describes a shrinkage, whereas changes in the negative direction result in an enlargement of the SCC. The extent of variation in the lateral canal is less compared to the posterior and superior canals. By looking at Fig. 5, PC2 affects the area where the superior and lateral canals converge. Moving in a positive direction leads to an enlargement of the posterior canal. PC1 and PC2 cause size variations in the vestibule area. From –2 to +2, the vestibule area results in a shrinking and vice-versa. PC3 mainly captures changes in the middle part of the lateral semicircular. PC4 primarily influences the area of the posterior semicircular canal and the superior semicircular canal. Looking at Figure 6, we can tell that the shape outlier S2 from the plot in Figure 5 has a large vestibule area and a large size of the canals.

3.4. Shape model evaluation

A substantial part of the creation of SSM is to validate the results. Intuitively a first qualitative approach is the visual inspection of the shape instances that the model is able to create. When shapes have point-to-point correspondence, an SSM is evaluated using more objective accepted measures, namely Generalization, Specificity, and

Compactness, which are considered as useful benchmarks for measuring correspondence quality [9, 22].

Figure 3(b,c,d) shows the evaluation of the SSM concerning compactness, generalization, and specificity with an increasing number of modes of variation included. Briefly, the generalization measures the model's ability to represent unseen shape instances of the class. It is performed using leave-one-out cross-validation reconstruction experiments. The generalization error is expected to decrease with an increasing number of model parameters. Specificity measures whether the model can generate instances of an object close to those presented in the training set. It is measured by generating a large number of N random instances (N = 1000 in our experiments) using different modes. For every new sample, compute the distance to the closest shape in the training set. The mean distance error is expected to increase with more parameters, as the increasing number of PCs gives more flexibility to shape reconstruction. The compactness of the model is the ability to use as few parameters as possible to represent more shape instances in the training sets. Compactness is defined as the cumulative variance of the M largest modes.

3.5. Reconstruction accuracy

The reconstruction accuracy of the model has been evaluated by computing the mean surface distance between approximated model instances and input segmentations to ensure that each shape in the training set is well represented. The landmarks of the shape model constitute a point cloud. To represent an instance of the training data, the point cloud should cover the important part of the shape. The original mesh is obtained from the distance transform created from the initial manual segmentation and then compared to a mesh reconstructed from the predicted PBM. We compute the Hausdorff distance (mm) that takes the max of these vertex-wise distances to return a single value as a measure of accuracy [15]. The results after computing the Hausdorff distance range from 1.15 to 4.91 mm. The mean surface-to-surface distance was 2.42 mm (0.87 Std. Dev.).

4. Discussion and conclusion

This study aimed to explore and analyze the shape variations of the vestibular system for further application of the electrode placement for VI. To control design and implant variables, having realistic and detailed computational models of the SCC are needed, including population variability. This work describes the first stage, having the model which can be used currently for design decision support of an implant.

An important aspect in this work was the use of data sets that are acquired in clinical practice. On the other hand, the quality of the data, especially the resolution and contrast of the scans and the accuracy of the manual segmentation, was a major concern. In some samples, the spacing between voxels is so low that the SCC consists of a single voxel across the entire diameter. In addition, due to the different voxel spacings for all images, resampling the volumes introduces even more artifacts. A challenge during the construction of the shape models is the methodology for creating point correspondences between the data. The initial shape model contained imperfections due to bad correspondences, which was alleviated with the application of a smoothing filter. Several experiments were carried out to establish the parameters to obtain an optimal SSM of the SCCs. Increasing the number of particles above 4096 does not significantly improve the shape representation of the model in the sense that no additional anatomical details become visible, but increases model complexity and computational time, especially when modeling such a complex structure as the vestibule and larger datasets. Therefore, a balance between a good representation and the number of particles is necessary. In general, the rest of the parameters involved in the optimization do not significantly affect the final model for this dataset.

The analysis of the shape variation based on the principal modes could help to find some outliers. Of course, it is mainly a proof-of-concept since the model is built with a small number of datasets, and therefore the representation of actual anatomy is not proved completely. Nevertheless, the accuracy tests have shown that the generated model based on the 71 segmentations approximated the shape of the vestibular system with reasonable accuracy. A lower generalization and specificity error is desirable for an ideal shape model, but Fig. 3(c, d) indicates that they move in opposite directions with an increasing number of model components. The compactness is also essential to guarantee that most of the shape variation is captured by the model using as few model parameters as possible. So how many components should be used to represent 90% or more of the shape variation is still a very interesting question when dealing with biological data, and a trade-off between these three metrics is necessary. In our model, 17 PCs are sufficient to represent 90% of the variation. For representing more than 95%, the gains in compactness and generalization are very light after 30 PCs, and there is a diminishing penalty in specificity as the number of components in the model increases. This flattening of the curve mainly occurs between 20 and 30 components. With more than 30 components used, the model constructed has the best performance, but also more noisy shape variation is introduced, and more computation is required to fit our models.

References

[1] Dean C. Barratt, Carolyn S.K. Chan, Philip J. Edwards, Graeme P. Penney, Mike Slomczykowski, Timothy J. Carter, and David J. Hawkes. Instantiation and registration of sta-

tistical shape models of the femur and pelvis using 3d ultrasound imaging. *Medical Image Analysis*, 12(3):358–374, jun 2008.

[2] Andrew P. Bradshaw, Ian S. Curthoys, Michael J. Todd, John S. Magnussen, David S. Taubman, Swee T. Aw, and G. Michael Halmagyi. A mathematical model of human semicircular canal geometry: A new basis for interpreting vestibular physiology. *Journal of the Association for Research in Otolaryngology*, 11(2):145–159, 6 2010.

[3] Joshua Cates, Shireen Elhabian, and Ross Whitaker. Chapter 10 - shapeworks: Particle-based shape correspondence and visualization software. In *Statistical Shape and Deformation Analysis*, pages 257–298. Academic Press, 3 2017.

[4] Joshua Cates, P. Thomas Fletcher, Martin Styner, Heather Cody Hazlett, and Ross Whitaker. Particle-based shape analysis of multi-object complexes. In *Medical Image Computing and Computer-Assisted Intervention – MICCAI 2008*, volume 5241, pages 477–485. Springer Berlin Heidelberg, 2008.

[5] Joshua Cates, P. Thomas Fletcher, Martin Styner, Martha Shenton, and Ross Whitaker. Shape modeling and analysis with entropy-based particle systems. In *Information Processing in Medical Imaging*, pages 333–345. Springer Berlin Heidelberg, 2007.

[6] Juan Cerrolaza, Sergio Vera, Alexis Bagué, Mario Ceresa, Pablo Migliorelli, Marius George Linguraru, and Miguel Ángel González Ballester. Hierarchical shape modeling of the cochlea and surrounding risk structures for minimally invasive cochlear implant surgery. In *Clinical Image-Based Procedures. Translational Research in Medical Imaging*, pages 59–67. Springer International Publishing, 2014.

[7] T.F. Cootes, C.J. Taylor, D.H. Cooper, and J. Graham. Active shape models-their training and application. *Computer Vision and Image Understanding*, 61(1):38–59, jan 1995.

[8] Iván Cortés-Domínguez, María A. Fernández-Seara, Nicolás Pérez-Fernández, and Javier Burguete. Systematic method for morphological reconstruction of the semicircular canals using a fully automatic skeletonization process. *Applied Sciences*, 9(22):4904, nov 2019.

[9] Rhodri Huw Davies. *Learning shape: optimal models for analysing natural variability*. PhD thesis, University of Manchester Manchester, 2002.

[10] Thomas Demarcy. *Segmentation and study of anatomical variability of the cochlea from medical images*. PhD thesis, Université Côte d'Azur, 2017.

[11] K. D. Fritscher, P. F. Raudaschl, M. Handler, C. Baumgartner, L. Johnson, A. Schrott-Fischer, R. Glueckert, R. Saba, and R. Schubert. Towards a framework for thesegmentation and statistical shape analysis of the vestibular system using micro-ct. In *Shape Symposium 2015, Delémont, Switzerland*, 2015.

[12] Nicolas Gerber, Mauricio Reyes, Livia Barazzetti, Hans Martin Kjer, Sergio Vera, Martin Stauber, Pavel Mistrik, Mario Ceresa, Nerea Mangado, Wilhelm Wimmer, Thomas Stark, Rasmus R. Paulsen, Stefan Weber, Marco Caversaccio, and Miguel A.González Ballester. A multiscale imaging and modelling dataset of the human inner ear. *Scientific data*, 4(1):1–12, 2017.

[13] Nils Guinand, Frans Boselie, Jean-Philippe Guyot, and Herman Kingma. Quality of life of patients with bilateral vestibulopathy. *Annals of Otology, Rhinology & Laryngology*, 121(7):471–477, 7 2012.

[14] Jean-Philippe Guyot and Angelica Perez Fornos. Milestones in the development of a vestibular implant. *Current Opinion in Neurology*, 32(1):145–153, feb 2019.

[15] D.P. Huttenlocher, G.A. Klanderman, and W.J. Rucklidge. Comparing images using the hausdorff distance. *IEEE Transactions on Pattern Analysis and Machine Intelligence*, 15(9):850–863, 1993.

[16] Hans Martin Kjer, Jens Fagertun, Sergio Vera, Miguel Angel González Ballester, and Rasmus Reinhold Paulsen. Shape modelling of the inner ear from micro-ct data. In *Shape Symposium*, volume 1992, 2014.

[17] J. H. Noble, R. F. Labadie, O. Majdani, and B. M. Dawant. Automatic segmentation of intracochlear anatomy in conventional ct. *IEEE Transactions on Biomedical Engineering*, 58(9):2625–2632, 9 2011.

[18] NORD. Benign paroxysmal positional vertigo. `https://rarediseases.org/rare-diseases/benign-paroxysmal-positional-vertigo`, 2020. Accesed 23 September 2021.

[19] Patrik Raudaschl and Karl Fritscher. Statistical shape and appearance models for bone quality assessment, 2017.

[20] G.K. Rohde, A. Aldroubi, and B.M. Dawant. The adaptive bases algorithm for intensity-based nonrigid image registration. *IEEE Transactions on Medical Imaging*, 22(11):1470–1479, nov 2003.

[21] Julia A. Schnabel, Daniel Rueckert, Marcel Quist, Jane M. Blackall, Andy D. Castellano-Smith, Thomas Hartkens, Graeme P. Penney, Walter A. Hall, Haiying Liu, Charles L. Truwit, Frans A. Gerritsen, Derek L. G. Hill, and David J. Hawkes. A generic framework for non-rigid registration based on non-uniform multi-level free-form deformations. In *Medical Image Computing and Computer-Assisted Intervention – MICCAI 2001*, pages 573–581. Springer Berlin Heidelberg, 2001.

[22] Martin A. Styner, Kumar T. Rajamani, Lutz-Peter Nolte, Gabriel Zsemlye, Gábor Székely, Christopher J. Taylor, and Rhodri H. Davies. Evaluation of 3d correspondence methods for model building. In *Information Processing in Medical Imaging*, volume 2732, pages 63–75. Springer Berlin Heidelberg, 2003.

[23] Daniel Q. Sun, Bryan K. Ward, Yevgeniy R. Semenov, John P. Carey, and Charles C. Della Santina. Bilateral vestibular deficiency: quality of life and economic implications. *JAMA Otolaryngology–Head & Neck Surgery*, 140(6):527, 6 2014.

[24] Michael von Brevern and Hannelore Neuhauser. Epidemiological evidence for a link between vertigo and migraine. *Journal of Vestibular Research*, 21(6):299–304, 2011.

[25] Matthias Willenbrink. Segmentation of the vestibular organ with statistical shape models and deep neural networks. Master's thesis, UMIT Private Universität für Gesundheitswissenschaften, Medizinische Informatik und Technik GmbH, 2021.

[26] Jennifer Wipperman. Dizziness and vertigo. *Primary Care: Clinics in Office Practice*, 41(1):115–131, mar 2014.